Conductance of a conjugated molecule with carbon nanotube contacts

Nicolas A. Bruque,[1,*] M. K. Ashraf,[1] Gregory J. O. Beran,[2] Thomas R. Helander,[3] and Roger K. Lake[1,3]
[1]*Department of Electrical Engineering, University of California–Riverside, Riverside, California 92521, USA*
[2]*Department of Chemistry, University of California–Riverside, Riverside, California 92521, USA*
[3]*Department of Computer Science and Engineering, University of California–Riverside, Riverside, California 92521, USA*
(Received 12 June 2008; revised manuscript received 14 September 2009; published 29 October 2009)

The conductance of an experimentally measured metallic carbon nanotube (CNT)-molecule-CNT structure is calculated. The features in the predicted transmission correspond directly to the features of the isolated molecular orbitals and surface states of the cut ends of the CNTs. The highest occupied molecular orbital (HOMO) provides a weakly coupled conductive channel with transmission features that are qualitatively insensitive to the chemical end groups of the cut CNTs, the cut angle, the CNT chirality, and the number of molecular bridges. Quantitatively, however, these factors can modify the resonance width by an order of magnitude giving rise to corresponding changes in the resistance. Furthermore, the cut ends of a zigzag CNT can have surface states which hybridize with the molecular HOMO state giving a large transmission peak at the Fermi level. To understand the molecular energy-level alignment with the CNT Fermi level, a quantum chemical calculation of the ionization potential and electron affinity and a density-functional theory calculation of the CNT image potential are performed. A twist on molecular conformation-change switching is also suggested.

DOI: 10.1103/PhysRevB.80.155455 PACS number(s): 73.63.−b, 85.65.+h, 05.60.Gg, 71.15.Mb

I. INTRODUCTION

Individual molecules have been proposed as the ultimately scaled electronic device in future electronics.[1–6] From an electronic device point of view, carbon nanotube (CNT) contacts to molecules have been shown to be superior to metal contacts both theoretically[7,8] and experimentally.[9] Recently, CNTs have been used to contact single molecules.[10–13]

Prior studies examining model CNT-molecule-CNT structures find that molecular transport is influenced by the chirality of the CNT contacts.[14–16] Others report changes when examining the passivation chemistry at the cut ends of the CNTs (Ref. 17) and the spatial gap between CNT contacts.[18] In this paper, we describe our theoretical study of an experimentally built CNT-molecule-CNT system described in (Ref. 12).

Obtaining agreement between experimentally measured currents and density-functional theory (DFT) transport calculations of metal-molecule-metal systems is difficult. DFT calculations do not give quantitatively accurate highest occupied molecular orbital (HOMO) and lowest unoccupied molecular orbital (LUMO) levels,[19–26] and they do not include the potential on the molecule resulting from the surface polarization of the metal (i.e., the image potential).[19,22,27] This results in an incorrect alignment of the molecular levels with the Fermi levels of the contacts.[19,28–30] Several studies have addressed these limitations by correcting the DFT energy of the molecular states.[22,29] Neaton *et al.* performed a quasiparticle GW correction to the DFT energies to take into account the polarization effect of the gold substrate upon physisorbing the molecule.[22] The study showed that the resulting energy shifts could be well approximated by considering separate calculations of the molecular ionization potential (IP), the electron affinity (EA), and the image potential and then treating these values as corrections or 'self-energies' to shift the DFT levels. This correction scheme was applied to the calculation of the conductance of benzene connected to gold through an amine linker, and it was shown to lower the traditionally too-large conductance value obtained from DFT to a value that agreed well with the experimental data.[19] For the CNT-molecule-CNT system, we proceed in the same fashion to understand the energy-level alignment between the molecular orbitals and the Fermi levels of the CNT leads.

Agreement between theory and experiment is further complicated by the fact that the exact structure tested is not known. Unknowns are the chirality of the CNT, the angle of the cut ends that connect to the molecule, the passivation chemistry of the cut ends, the number of molecules connecting the CNTs, and the angle/site at which they connect. Therefore, to compare theoretical calculations with experimental measurements, one must simulate a number of probable structures to understand how different variations of the structure affect the conductance.

II. METHOD

Four different types of calculations are performed. (1) The entire CNT-molecule-CNT structure is relaxed using the DFT, tight-binding, molecular-dynamics code FIREBALL.[31–35] (2) Once the structure is relaxed, the Hamiltonian and overlap matrix elements are taken from FIREBALL and used in a nonequilibrium Green's-function (NEGF) algorithm to calculate transmission.[36] (3) The image potential is calculated by placing a positive charge between the two CNTs and performing a self-consistent FIREBALL/NEGF calculation of the charge on the CNTs using a recursive Green's-function algorithm (RGF). (4) The molecular IP and EA are evaluated by computing the gas-phase energies of the neutral, cation, and anion molecule. Both vertical and adiabatic ionization potentials are determined. Below, these different calculations are described in detail.

A. Structure relaxation

1. FIREBALL

Structure relaxation is performed with the DFT code FIREBALL. Separable, nonlocal Troullier-Martins pseudopotentials and the BLYP exchange-correlation functional are used.[37–39] The foundation of the FIREBALL method is a self-consistent generalization of the Harris-Foulkes energy functional[40,41] known as DOGS, labeled after the initials of original authors.[32,33,35] In the self-consistent evaluation of the total energy, the charge density is based on the sum of confined atomiclike densities $\rho(\mathbf{r})=\Sigma_i n_i|\phi_i(\mathbf{r}-\mathbf{R}_i)|^2$ where n_i is the occupation of localized orbital ϕ_i centered at $\mathbf{R}_i$.[32] These orbitals are slightly excited due to hard wall boundary conditions imposed at certain radial cutoffs r_c for each atomic species. The cutoffs are determined by an excitation energy of approximately 2.0 eV thereby preserving the chemical bonding trends. In this study, we use the following s-orbital and $p_{x,y,z}$-orbital cutoff values: $r_c^{1s}=4.10$ Å for hydrogen; $r_c^{2s}=4.4$ Å and $r_c^{2p}=4.8$ Å for carbon; $r_c^{2s}=4.0$ Å and $r_c^{2p}=4.4$ Å for nitrogen; $r_c^{2s}=3.7$ Å and $r_c^{2p}=4.1$ Å for oxygen. All two and three center integrals are tabulated as functions of interatomic distances in advance and placed on interpolation grids. Molecular dynamics simulations are performed by looking up the integrals from the interpolation grids. Structures are relaxed until all Cartesian forces on the atoms are <0.05 eV Å^{-1}. A Fermi smearing temperature of 50 K and a self-consistent convergence factor of 10^{-5} are used. The one-dimensional Brillouin zone is sampled with 32 k points during optimization.

2. Structure

The CNT leads of the CNT-molecule-CNT system are metallic and approximately 1 nm in diameter. Both (7,7) and (12,0) CNTs are used. The CNT leads are attached to the π-cruciform molecule labeled as molecule 1 of Ref. 12. The molecule is covalently bonded to the CNTs via amide linkers. At the dodecyloxybenzene cross-arm ring ends, we attach a truncated C_2H_5 alkane chain instead of the $C_{12}H_{25}$ used in the experiment. Since the alkane chain has a wide HOMO-LUMO gap, this substitution should not affect the electronic states of the planar, conjugated molecule near the Fermi level. An example is shown in Fig. 1(a) using armchair (7,7) CNT contacts.

To construct this structure, we first construct the isolated planar molecule with amide groups attached at both ends. The amides are terminated by hydrogen. This isolated molecule is relaxed in gas-phase using FIREBALL.

To create the CNT leads, we begin with one DFT optimized CNT block layer composed of 4 atomic layers. We copy and repeat the CNT block layer in the axial direction. A length of the middle section of the CNT that most closely corresponds to the length of the molecule is removed. We assume that after the etching step, the CNT contacts are fixed in their position and the molecular window is governed by the one-dimensional atomic-layer spacing of the CNTs.[10–12] We find that 18 atomic layers (22.4 Å) of an armchair or zigzag CNT is comparable in length to the relaxed molecule plus amide groups. The cut ends of the CNTs are passivated with either hydrogen atoms or carboxyl groups.

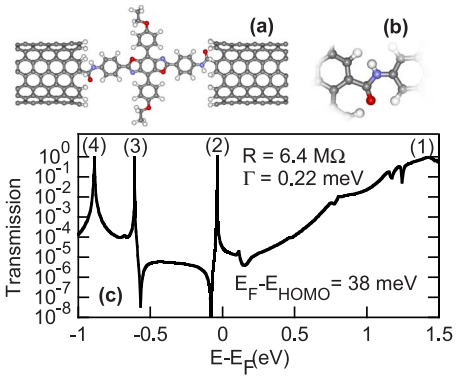

FIG. 1. (Color online) (a) Relaxed CNT-molecule-CNT structure with armchair (7,7) CNT contacts. (b) Close-up of CNT-amide bond relaxed configuration. (c) Calculated transmission of the armchair CNT-molecule-CNT structure.

Eight CNT block layers (32 atomic layers) for each contact are long enough to damp out charge oscillations at the outside end layers that result from the C-H charge dipoles at the cut interfaces.[36] The CNT contacts are at least ten block layers (4 nm) in length from the molecule interface to each supercell edge. The relaxed molecule plus linkers is attached to the cut CNT ends. The entire supercell is relaxed using periodic boundary conditions. The Hamiltonian matrix elements of this structure are used for calculating the equilibrium transmission and conductance as described further in Sec. II B.

B. Transmission and conductance

The Hamiltonian matrix elements of the relaxed structure are used in the NEGF algorithm to calculate the surface self-energies, Green's function of the device, and the resulting transmission. The surface self-energies for the left and right open boundaries, $\mathbf{\Sigma}^{\ell}$ and $\mathbf{\Sigma}^{r}$, are calculated using the matrix elements of the end layers of the relaxed supercell. These matrix elements are used in a decimation algorithm as described in.[36,42,43] The retarded Green's function is calculated from $\mathbf{G}^R(E)=[E\mathbf{S}_D-\mathbf{H}_D-\mathbf{\Sigma}^{\ell}-\mathbf{\Sigma}^{r}]^{-1}$ where E is the energy, $\mathbf{S}_D$ is the overlap matrix of the device, and $\mathbf{H}_D$ is the Hamiltonian matrix of the device. The "device" is defined as the finite region between the two open boundaries. Bold font is used to indicate that a quantity is a matrix.

The transmission spectrum, $T(E)$, is calculated from the standard Green's-function expression,

$$T(E)=\mathrm{tr}\{\mathbf{\Gamma}_{1,1}\mathbf{G}^R_{1,N}\mathbf{\Gamma}_{N,N}(\mathbf{G}^R_{1,N})^{\dagger}\}, \tag{1}$$

where indices 1 and N in Eq. (1) indicate the first and last block layers of the left and right CNT leads, respectively, $\mathbf{\Gamma}_{1,1}=i(\mathbf{\Sigma}^{\ell}-\mathbf{\Sigma}^{\ell\dagger})_{1,1}$, and $\mathbf{\Gamma}_{N,N}=i(\mathbf{\Sigma}^{r}-\mathbf{\Sigma}^{r\dagger})_{N,N}$. Note that $\mathbf{\Sigma}^{\ell}$ and $\mathbf{\Sigma}^{r}$ are, by construction, nonzero only in blocks 1,1 and N,N, respectively.

The current is obtained from

$$I = \frac{2e}{\hbar}\int \frac{dE}{2\pi}T(E)[f(E-\mu_L)-f(E-\mu_R)], \tag{2}$$

where $f(E)$ is the Fermi function, and μ_L and μ_R are the electrochemical potentials of the left and right contacts, respectively. The zero-bias conductance is calculated from the derivative of the current with respect to the voltage,

$$G = \frac{\partial I}{\partial V} = \frac{2e^2}{\hbar}\int \frac{dE}{2\pi}T(E)\left(-\frac{\partial f(E-E_f)}{\partial E}\right), \tag{3}$$

where E_f is the Fermi energy. The temperature is 300 K for all of the current and conductance calculations presented in this paper. Further details of our approach can be found in Ref. 36.

C. Calculation of the image potential

1. Image potential

When an electron or hole transfers from the CNT leads to the molecule, it will reside on the molecule for a period of time corresponding to the resonant state lifetime, τ. During this time, the electron or hole will induce an image charge in the CNTs and a polarization charge in the SiO_2 substrate. This induced charge results in an image potential which modifies the energy of the resonant state.

For the calculation of the image potential resulting from the induced charge on the CNTs, we extend the left and right CNT contact leads of the relaxed supercell by copying and repeating both left and right outside CNT block layers. We lengthen both CNT contact ends to 10 nm giving a total length of approximately 22 nm for the entire structure. This ensures that the electric field from the point charge is well screened at the left and right boundaries. We remove the molecule and terminate the connection points on the CNTs with H. Then we add a point charge at the position $\vec{r}_0$ corresponding to the center of the molecular HOMO level. The structure used for the calculation is shown in Fig. 2(a).

The potential resulting from the point charge is $-qV(\vec{r}) = \frac{-q^2}{4\pi\epsilon_0|\vec{r}-\vec{r}_0|}$, and the Hamiltonian matrix elements resulting from that potential are approximated as

$$\mathbf{U}_{i,j} = \frac{-q^2}{8\pi\epsilon_0}\left[\frac{1}{|\vec{r}_i-\vec{r}_0|}+\frac{1}{|\vec{r}_j-\vec{r}_0|}\right]\mathbf{S}_{i,j}, \tag{4}$$

where i and j index the atoms at positions $\vec{r}_i$ and $\vec{r}_j$, q is the charge of an electron, and ϵ_0 is the permittivity of free space.

Once the charge occupation for the system converges with the added point charge, the electrostatic potential is evaluated across the junction in the plane of the molecule, along a series of points $\vec{r}_p$, using

$$\Phi(\vec{r}_p) = \sum_i \frac{(-q)(n_i-n_i^0)}{4\pi\epsilon_0|\vec{r}_p-\vec{r}_i|}, \tag{5}$$

where $-qn_i$ is the valence charge associated with atom i, $-qn_i^0$ is the neutral atom charge, and $\vec{r}_i$ is the atomic position for every atom i of the two CNTs including the H atoms. Note that this sum does not include the point charge between the CNTs. The same self-consistent calculation is performed for the cut, H-passivated CNT in the absence of the extra point charge, and the potential across the gap for this system Φ^0 is also calculated using Eq. (5). The difference, $\Phi(\vec{r}_0) - \Phi^0(\vec{r}_0)$, gives the image potential Φ_{CNT}.

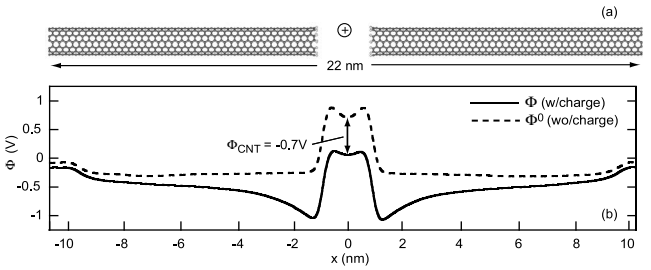

FIG. 2. (a) Structure used for the calculation of the image potential. The molecule is removed and the connecting C atoms of the CNTs are terminated with H. A positive point charge is placed at a point corresponding to the center of the molecule. The open boundaries at the left and right CNT ends are included via self-energies, and the charge is calculated with the recursive Green's function algorithm. (b) Potential profiles Φ (solid) and Φ^0 (dashed) plotted along an axial line that lies on top of the CNT contacts and passes through the center of the point charge. The image potential at $x=0$ is used to renormalize the HOMO energy level. The small potential steps at ± 10 nm are the result of the boundary conditions described in the text.

For comparison and verification, we also model the image charge of a CNT-vacuum-CNT system by discretizing two grounded cylinders of sheet charge, assuming cylindrical symmetry, where each cylinder is 50 nm long and 1 nm in diameter. The cylinders are separated by 2 nm matching the molecular window used for the planar molecule between armchair CNTs. A point charge is placed between the 2 cylinders on the longitudinal axis. The induced charge on the cylinders is solved by the method of moments.[44] The potential between the cylinders is calculated from the equivalent of Eq. (5) where i indexes the discretized site, $n_0=0$, and $-qn_i$ is the charge on discretized site i.

There is also an image potential resulting from the discontinuity in the dielectric at the SiO_2 interface. The image potential due to a charge q in medium 1 a distance d above medium 2 is $\Phi_d = \frac{-q}{4\pi\epsilon_1(2d)}\frac{\epsilon_2-\epsilon_1}{\epsilon_2+\epsilon_1}$ where ϵ_1 and ϵ_2 are the dielectric constants in mediums 1 and 2, respectively. Letting medium 1 be air, medium 2 be SiO_2 with a relative dielectric constant of 3.9, $d=1$ nm, and q be a positive hole charge, $\Phi_d=-0.43$ V.

2. Electron density

Using the self-consistent field loop of the DFT code FIREBALL to perform the calculation of $\Phi-\Phi^0$ results in some ambiguity since the addition of the positive charge shifts the Fermi level of the dual CNT system. Therefore, for this calculation, we replaced the FIREBALL charge calculation based on a sum of eigenvectors with a NEGF charge calculation. A NEGF charge calculation allows us to fix the Fermi level to that of the bulk CNT. Experimentally, the Fermi level is fixed by the unperturbed semi-infinite CNT leads. The potential in the vicinity of the charge shifts, but the Fermi level remains fixed.

To ensure that the electric field is well screened at the outer boundaries, the left and right CNT leads are each extended to 10 nm. This results in a Hamiltonian matrix which is too large to store and invert directly. Therefore, we obtain the diagonal and first off-diagonal blocks of $\mathbf{G}^R(E)=[E\mathbf{S}_D-\mathbf{H}_D-\mathbf{\Sigma}^\ell-\mathbf{\Sigma}^r]^{-1}$ using the recursive Green's-function algorithm. For this particular work, we have only used it to calculate the charge induced on the CNTs in response to a point charge placed between them. The full description of the algorithm is given in the Appendix.

D. Ionization potential and electron affinity

Typically, density functional theory is used to model large molecules because of its general accuracy and low computational cost. However, both the DFT HOMO and LUMO levels frequently differ markedly from experimental results (see, for example, Refs. 24–26). Therefore, we estimate the HOMO/LUMO levels and the quasiparticle gap relevant to electron and hole transport by calculating the gas-phase IP and EA of the gas-phase molecule that links the CNTs.[22] For the large molecule of this study, all IP and EA energy calculations are performed using the DFT package Q-CHEM 3.1 (Ref. 45) using the Perdew-Burke-Ernzerhof (PBE) [generalized gradient approximation (GGA)] density functional and the 6-311+$G(3df,2p)$ basis set. The geometry optimizations are performed in the 6-31+$G(d,p)$ basis.[46–48] The zero-point energy is not included. In all optimizations, the ends of the molecules are constrained to mimic attachment to fixed CNT leads. A study of small-molecule ionization potentials and electron affinities found absolute mean (max) PBE errors of 0.16 (0.5) and 0.11 eV (0.3 eV) relative to experiment.[49] From these results, we estimate the error bars on our predictions to be roughly 0.5 and 0.3 eV for the IP and EA, respectively.

Two possible definitions of IP and EA exist, vertical and adiabatic. The vertical IP and EA are evaluated by computing the energies of the neutral, cation, and anion molecules at the neutral-molecule geometry. The adiabatic quantities are computed from the anion and cation energies at their respective optimized gas-phase geometries. If the lifetime of the resonant state is short relative to the time scale of molecular relaxation ($\sim 10^{-13}-10^{-14}$ s), no nuclear relaxation occurs and the electron transport can be viewed as an electronic process (i.e., vertical excitation). On the other hand, if the resonant state lifetime is longer, the molecule can be expected to undergo both nuclear and electronic relaxation, in which case an adiabatic model is more appropriate. The resonant state lifetime τ can be estimated from the full width half maximum (FWHM) of the resonances in the transmission according to FWHM$=\hbar/\tau$.

III. RESULTS AND DISCUSSION

First we will present results from DFT/NEGF calculations of the transmission for several physical implementations of the CNT-molecule-CNT system. We will show the effect of CNT chirality, passivation chemistry, cut angle, and multiple molecules on the transmission spectrum. Then we will consider the energy-level alignment between the molecular HOMO and LUMO levels and the Fermi level of the CNTs.

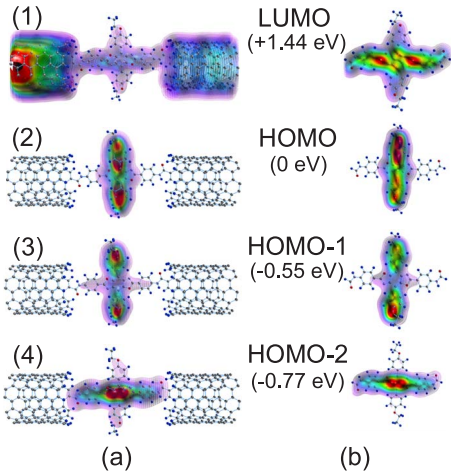

FIG. 3. (Color online) (a) Three-dimensional contour plots of the covariant spectral function corresponding to the resonant peaks marked in Fig. 1. (b) Corresponding molecular orbitals for the relaxed isolated molecule in the planar conformation. Amide groups are included at the left and right ends of each molecule.

A. Transmission and conductance

1. Armchair CNTs, H-passivation, and single molecule

We first examine the transport characteristics of an armchair CNT-molecule-CNT system shown in Fig. 1(a). The *C* sites along the edge of the armchair CNTs, shown in Fig. 1(b), have bonding angles that allow us to initially orient the plane of the molecule parallel to the tangential plane of the CNT at the point of contact. The system remains stable during the DFT relaxation, and the dihedral angle between the plane of the amide groups and the tangential plane of the CNTs at the point of contact changes by no more than 14.1° from parallel after relaxation.

In Fig. 1(c), we show the calculated transmission spectrum of the armchair CNT-molecule-CNT system as a function of the difference $E-E_F$. The transmission of the molecule has a resonant peak 38 meV below the Fermi energy, [E_F-E_{HOMO})] which results in a room-temperature (300 K) resistance of 6.4 MΩ. The resonant peak has a FWHM (Γ) equal to 0.22 meV. For reference, the experimentally measured resistance is 5 MΩ.[12]

To understand the transmission curve we compare the covariant spectral functions,[36] shown in Fig. 3(a) to the molecular orbitals of the molecule in vacuum in Fig. 3(b). The spectral-function labels (1–4) correspond to the labeled transmission peaks in Fig. 1(c). The energies listed in eV next to the molecular orbitals are the differences in energy of the molecular orbitals in vacuum with respect to the molecular HOMO in vacuum.

Broad transmission peak (1) corresponds to the LUMO with a spectral function that is spread across both the CNTs and the molecule. The broad peak in transmission indicates that the coupling of the CNT states to the molecular LUMO is strong, which is consistent with the large spatial spread of

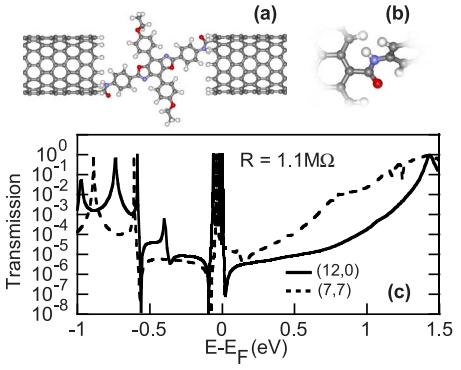

FIG. 4. (Color online) (a) Relaxed CNT-molecule-CNT structure with zigzag (12,0) CNT contacts. (b) Close-up of CNT-amide bond configuration. (c) Calculated transmission of the zigzag CNT-molecule-CNT structure (solid) and the armchair CNT-molecule-CNT structure (dashed).

the spectral function across both the molecule and the CNTs.

Peak (2) in the transmission curve results from the coupling of the CNT states to the HOMO. The HOMO is localized on the cross arm of the molecule away from the CNTs and is weakly coupled to the contacts. The narrowness of the HOMO transmission peak is the result of two things. (i) The molecular orbital is spatially localized away from the CNTs, and (ii) the spectral weights near and on the C atom part of the amide linkers are low. We note that the effect of the amide linkers is consistent with previous studies which also found that amide linkers reduce the coupling of the CNT states to the molecular HOMO orbital.[14,15] The Fano resonance at peak (2) results from the two parallel paths through the molecule. An electron can tunnel through the tail of extended state (1) or it can tunnel through localized state (2).

Transmission peak (3) corresponds to the HOMO-1 state, approximately −0.5 eV below the HOMO, peaked on oxygen atoms of the upper and lower portions of the cross arm. Transmission peak (3) is also a Fano resonance arising from the two parallel paths corresponding to the HOMO-1 state localized on the cross arms and the HOMO-2 state extended across the molecule.

Although the LUMO and HOMO-2 levels extend across the molecule, the resonance due to HOMO-2 is sharp compared to that of the LUMO. The narrowing of the HOMO-2 resonance compared to the LUMO is again consistent with other studies using amide linkers.[14,15]

2. Zigzag CNTs, H-passivation, and single molecule

To investigate how the contact chirality affects transport, we attach (12,0) CNT contacts approximately 1 nm in diameter to the molecule shown in Fig. 4(a). The axial direction of the C-H bonds at the cut ends of the CNTs prevents us from attaching the molecule directly across the junction, parallel to the CNT axis. Instead, the molecule is attached across the CNTs with attachment points $4\frac{1}{2}$ H atoms apart. The fraction $\frac{1}{2}$ comes about because the cut ends of the left and right CNT differ by one atomic layer. A close up of one attachment is shown in Fig. 4(b). This configuration forces some twisting of the amide linkers with respect to the molecule and the CNTs. The relaxed dihedral angle between the amide linker and tangential plane of the CNT at the point of contact is 43° on the left and 32° on the right. The relaxed dihedral angle between the amide linker and plane of the molecule is 19° on the left and 26° on the right.

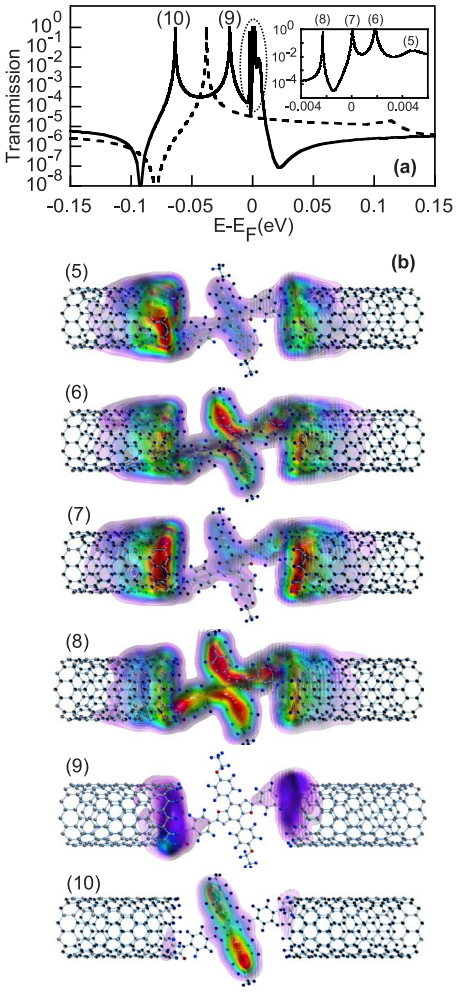

FIG. 5. (Color online) (a) Calculated transmission close to the Fermi energy where the solid line represents the zigzag system and the dashed line represents the armchair system. (b) The spectral functions corresponding to the resonant transmission peaks marked in (a) for the zigzag CNT-molecule-CNT structure. Inset shows peaks clustered above and below E_F=0 eV

Figure 4(c) shows the transmission spectrum of the CNT-molecule-CNT structure with (12,0) zigzag CNT contacts (solid line) overlaid on the transmission spectrum from Fig. 1(c) (dashed line). The important difference between the two curves is the splitting of the HOMO transmission peak into multiple split transmission peaks near the Fermi energy. The splitting results from the HOMO state interacting with H passivated surface states at the CNT interface. This results in a room-temperature (300 K) resistance of 1.1 MΩ.

Figure 5(a) provides a closer look at the transmission near the Fermi energy where the solid and dashed lines are replotted from Fig. 4(c) over a small range of energy near E_F. The inset figure shows the cluster of peaks marked by a dashed circle near E_F. Here we see two peaks below and above the Fermi energy. The covariant spectral functions corresponding

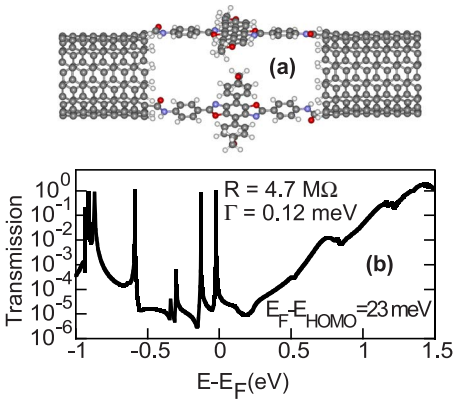

FIG. 6. (Color online) (a) Relaxed armchair CNT-molecule-CNT structure with two planar molecules attached. (b) Calculated transmission of CNT-molecule-CNT system shown in (a).

to each of the transmission peaks, labeled (5) through (10) are shown in Fig. 5(b). The single peak observed using armchair contacts splits into 6 peaks when zigzag contacts are used. The peaks result from the interaction of the molecular HOMO state, the surface states of the left CNT, and the surface states of the right CNT. This is clearly seen in the spectral-function plots. Multiple, nearly degenerate, surface states immediately above and below E_F on finite length, H-passivated, zigzag CNTs have been observed by others.[50]

The states shown in Fig. 5(b) labeled (5)–(8) corresponds to a mixture of two surface states and the molecular HOMO. The middle state labeled (9) is a mixture of two surface states. The lowest state labeled (10) is primarily the molecular HOMO, and its transmission resonance has a FWHM of Γ=0.27 meV very similar to the HOMO resonance with armchair leads. Thus, surface states of the zigzag CNTs occur at and near the Fermi level, and their interaction is mediated and enhanced by the proximity of the molecular HOMO energy level. This gives rise to large transmission at the Fermi level. This enhancement of transmission through different conjugated molecules at the Fermi level with both H-passivated and unpassivated zigzag CNT leads has also been observed by others.[14,16]

The results shown in Figs. 1–4 show that for both the metallic armchair and zigzag CNT-molecule-CNT structures, the transmission is directly mapped to the features of the isolated molecular orbitals and the surface states of the cut ends of the CNTs.

3. Two molecules

Experimentally, it has been suggested that up to two molecular bridges might be established across the gap during the dehydration reaction.[12] To model such a system, we attach one additional molecule to our initial optimized armchair CNT-molecule-CNT structure and perform a DFT relaxation. Figure 6(a) shows the relaxed armchair CNT-molecule-CNT system where an additional planar molecule is attached parallel to the original molecule shown in Fig. 1(b). The maximally separated configuration of the two molecules shown here is known to be energetically favorable.[17]

The two molecule transmission is shown in Fig. 6(b) where we observe a doubling of peaks near the Fermi level giving a calculated resistance of 4.7 MΩ. As expected, the peaks are again associated with the same orbitals previously discussed and shown in Fig. 3. The addition of one molecular bridge reduces the resistance, but not by a factor of two. The resistance is sensitive to the position of the HOMO resonant transmission peaks with respect to the Fermi level. The two peaks from the two molecules split and shift compared to the single peak from a single molecule.

4. Passivation chemistry and cut angle

While the molecular end groups on the cut ends of the CNTs are not known, it is reasonable to assume that the CNT ends remain functionalized with carboxyl groups (COOH), rather than H atoms after the dehydration reaction.[12] However, we note that passivating an armchair CNT cut edge completely with carboxyl groups is not possible due to steric hindrance. Other end groups are possible,[51] however, in this work, we consider only COOH and H. We also note that attaching molecule 1 to a vertically cut armchair or zigzag CNT passivated with carboxyl groups results in a structure which is difficult to relax at the DFT level.

To mimic a complex CNT e-beam etch window, we cut a (7,7) armchair CNT nonvertically, along a zigzag edge leaving one armchair edge at the base of the cut. The structure is shown in Fig. 7(a). The thicker C and H atoms and bonds outlined in the top view mark the cut edge of the CNT side walls. The zigzag edges are passivated with carboxyl groups except for the two C atoms at the top of the cut. These two C atoms are passivated with hydrogen. Two carboxyl groups cannot be placed there due to steric hindrance. The molecule is attached at the bottom edge across the shortest portion of the gap. The relaxed planes of the amide linkers are no more than 24.2° from parallel to the tangential plane of the CNTs at the point of contact.

The transmission is shown in Fig. 7(c) by a solid line. The calculated resistance is 40 MΩ. The features remain qualitatively comparable to the features of the transmission in Fig. 1(c) where the spectral function at each peak again matches the features of the isolated molecular orbitals shown in Fig. 3. The LUMO and HOMO-2 peaks shift deeper into the conduction and valence bands, respectively. The position of the HOMO resonant peak is 14 meV below the Fermi level. For comparison, the peak of the HOMO resonance in Fig. 1(c) is 38 meV below the Fermi level. Quantitatively, we find a narrowing of the resonant peaks where the full width at half maximum (Γ_a) of the HOMO resonance is 0.023 meV. The narrowing of the valence-band resonances indicate less coupling of the molecular states to the continuum of states in the CNT contacts. Thus, the cause for the increased resistance of the structure compared to that of the structure in Fig. 1 is the result of the narrowing of the HOMO resonance by a factor of 9.

To determine if the passivation chemistry is affecting the resonant widths, we substitute H for each carboxyl group in the structure. We find that the hydrogen passivation narrows each resonance peak further which increases the resistance to 455 MΩ. This narrowing of the resonances due to H passi-

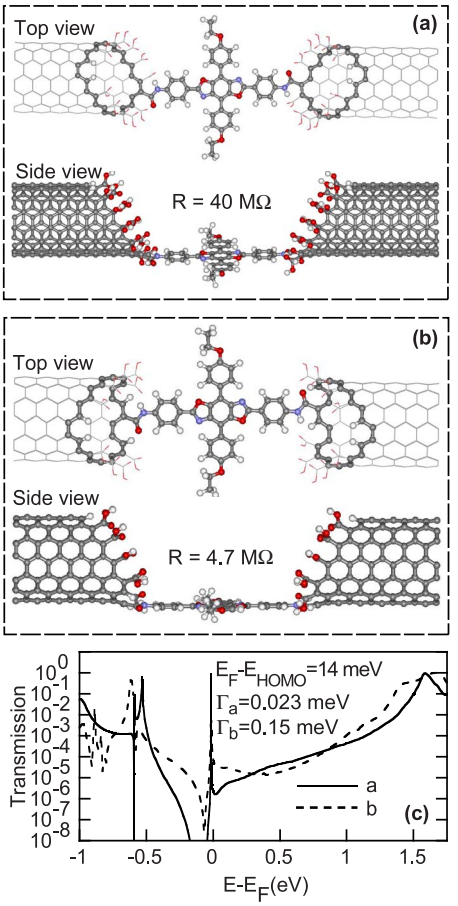

FIG. 7. (Color online) (a) Top and side views of a relaxed CNT-molecule-CNT structure with the CNT side walls passivated with carboxyl group molecules. Bolder atoms and bonds in top view represent the cut edge of the CNTs. (b) Top and side views of a relaxed CNT-molecule-CNT structure with the CNT side walls passivated with carboxyl/hydrogen molecules. Bolder atoms and bonds in top view represent the cut edge of the CNTs. (c) Calculated transmission of CNT-molecule-CNT systems shown in (a) (solid) and (b) (dashed).

vation is consistent with work done by Ren *et al.*[17] where passivated carboxyl groups were compared to H passivation on semiconducting (13,0) CNTs connected by a single diaminobenzene molecule.

Next, the cut shown in Fig. 7(a), is slightly modified to leave two armchair edges intact on either side of the molecule at the bottom of the cut. The modified interface and structure are shown in Fig. 7(b) where the top view thick atoms/bonds mark the CNT edge. We passivate the zigzag edges using carboxyl groups and use a mix of carboxyl groups and H for the remaining armchair edges. The molecule is positioned and oriented exactly as it is in the configuration shown in (a). We also note that the molecule to CNT interface connection is similar to the cut and chemistry configuration used in Fig. 1(b).

The transmission is shown in Fig. 7(c) by a dashed line. The energy of the transmission peak remains the same, however, the width of the HOMO resonance increases from 0.023 to 0.15 meV. The increase in coupling results in a decrease of resistance to 4.7 MΩ. A small change in the cut

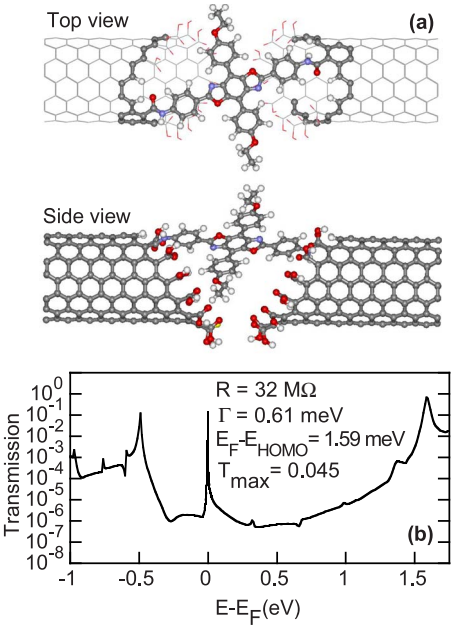

FIG. 8. (Color online) (a) Top and side views of a relaxed CNT-molecule-CNT structure with the CNT side walls passivated with carboxyl group molecules and the molecule attached on top. Bolder atoms and bonds in top view represent the cut edge of CNTs. (b) Calculated transmission of CNT-molecule-CNT systems shown in (a).

edge geometry results in nearly an order-of-magnitude change in the resistance. In this case, the change consisted of modifying the cut edge from zigzag to armchair in proximity to the molecule.

We consider a final cut and attachment geometry which results in asymmetric coupling of the HOMO level to the leads. We use the nonvertical cut geometry shown in Fig. 7(a) with the CNTs closer together so that the cut window is not wide enough to accommodate a molecule at the bottom of the cut, and the molecule attaches across the top of the gap. The structure is shown in Fig. 8(a). The relaxed molecule is attached via zigzag edges. All zigzag edges are passivated with carboxyl groups. Due to steric hindrance, we use H for the top zigzag edge and edges near the NH groups of the amide linkers.

The calculated transmission is shown in Fig. 8(b). The resistance is 32 MΩ. The features remain qualitatively comparable to the features of the transmissions in Fig. 7(c), however the position of the HOMO resonant peak has shifted to 1.59 meV below the Fermi level. For the first time, the maximum transmission of the HOMO resonance does not reach unity ($T_{\max}$=0.045). The FWMH of the HOMO transmission resonance is 0.61 meV. This decreased peak height is due to asymmetrical coupling of the left and right CNT contacts. The left contact dihedral angle between the molecule and tangential plane of the CNT is 12° and the right dihedral angle is 52°. Assuming a Lorentzian form for the resonance, the peak height and width give two equations for two unknowns, the energy broadening due to the left, Γ_L, and right, Γ_R, contacts. The FWHM $\Gamma=\Gamma_L+\Gamma_R$. Solving, we obtain Γ_L=0.598 meV and Γ_R=0.006 81 meV.

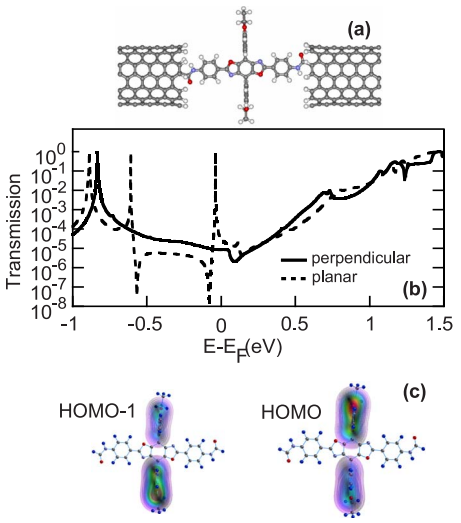

FIG. 9. (Color online) (a) Relaxed CNT-molecule-CNT structure with a perpendicular ethoxybenzene cross-arm conformation molecule attached. (b) Calculated transmission comparison where the solid line is for the system shown in (a) and the dashed line is for the planar ethoxybenzene cross-arm conformation shown in Fig. 1(a). (c) Molecular HOMO-1 and HOMO orbitals for the relaxed isolated molecule in the perpendicular conformation with amide groups attached.

For all three nonvertically cut CNT-molecule-CNT structures with carboxyl passivation, the transmission spectrum is qualitatively comparable to the transmission spectrum described in Secs. III A 1 and III A 2. There is a weakly coupled HOMO resonance appearing near the Fermi energy. However, changes in the passivation chemistry, the geometry of the cut, and the geometry at the point of connection of the molecule to the CNT do have a quantitative effect on the transmission and the resistance. The energetic position of the HOMO resonance varies by is less than $2k_BT$ at room temperature. The primary reason for the nearly order-of-magnitude change in the room-temperature resistance is the nearly order-of-magnitude change in the HOMO resonance width. These dependencies confirm that structural and chemical unknowns can cause significant variation of the resistance of the CNT-molecule-CNT system.

5. Molecular conformation

Lastly, we investigate how the molecular resonances are modified by changing the molecular conformation. We explore this by rotating the cross-arm ethoxybenzene rings in opposite directions. We find that only a planar and perpendicular gas-phase conformation is stable during relaxation with the planar conformation energetically favorable by 1.4 eV. Using the H-passivated, armchair CNT contacts, we relax the entire supercell using the perpendicular molecular conformation, resulting in the structure shown in Fig. 9(a).

The planar and perpendicular transmissions are shown in Fig. 9(b). The LUMO and HOMO-2 resonance peaks in both systems remain qualitatively the same. The HOMO-1 and HOMO transmission resonances, however, near the Fermi energy in the perpendicular configuration are removed. The absence of the HOMO transmission resonances gives a resistance of 1.6 GΩ. From the molecular-orbital plots shown in Fig. 9(c), we see that the HOMO and HOMO-1 are still localized on the cross-arm ethoxybenzene groups, however they are split in the middle and decoupled from the molecular bridge. The perpendicular conformation gas-phase HOMO and HOMO-1 levels appear nearly degenerate (0.02 eV difference) at 0.96 eV below the Fermi energy. For comparison the planar conformation gas-phase HOMO and HOMO-1 levels are 0.72 and 1.27 eV below the Fermi energy.

By rotating the ethoxybenzene rings we break the π-conjugation with the rings on the horizontal axis of the molecule thereby suppressing the HOMO and HOMO-1 level from the transmission spectrum. The HOMO and HOMO-1 levels associated with the cross arm are decoupled from the molecular bridge leaving no states near the Fermi energy to carry current. This results in an increase in resistance by over 2 orders of magnitude.

The use of conformation change for molecular switching is well known. Several examples are rotaxane,[52,53] 1,4-bis-phenylethynyl-benzene,[54] and 2′-amino-4-ethylphenyl-4′-ethylphenyl-5′-nitro-1-benzenethiolate,[55,56] which we refer to as the nitro molecule. In all cases the conformation change of the molecules alters the molecular orbitals along the path of the electron transport. In the nitro molecule, the conjugation is broken directly in the transport path between each contact. In rotaxane, the orbital changes from extended to localized along the transmission path of the molecule. For the cruciform molecule configurations, shown in Figs. 1(a) and 9(a), the effect of conformation is different. The rotation of the vertical rings does not affect the conjugation along the horizontal axis of the molecule, and it does not localize a previously extended state along the axis of the molecule. Instead, it decouples the HOMO from the transport path which results in an exponentially decreased transmission near the Fermi energy. This is a twist on the conformation-change paradigm of molecular switching from a three-terminal-device point of view.[11]

Results from all of the configurations discussed in Secs. III A 1–III A 5 are summarized in Table I.

B. Energy-level alignment

In all the different CNT-molecule-CNT configurations presented, the HOMO resonance provides a weakly coupled transport path through the planar molecule that is qualitatively insensitive to the interface orientation, CNT chirality, the number of molecular bridges, the molecule-CNT site connection or the termination chemistry. Overall the resistances of the planar molecule listed in Table I range from 1.1 to 40 MΩ. Because of the narrow resonance resulting from the weak coupling of the HOMO level to the CNTs, a shift of the HOMO level results in a change in conductance. Therefore, the relative position of the HOMO level with respect to the contact Fermi level is important for quantitative conductance calculations. To determine the HOMO energy level, we proceed by calculating the IP and EA of molecule 1 and the image potential resulting from a hole on the molecule.

TABLE I. Calculated resistance (R) (T=300 K), full width at half max (Γ), and HOMO resonant position relative to the CNT Fermi level ($\Delta E=E_F-E_{HOMO}$) of the seven CNT-molecule-CNT systems studied where "Planar" indicates the planar conformation of the molecule.

System	R (MΩ)	Γ (meV)	ΔE (meV)
Planar armchair, Fig. 1(a)	6.4	0.22	38
Planar zigzag, Fig. 4(a)	1.1		
Planar 2 molecules, Fig. 6(a)	4.7	0.12	23
Planar carboxyl, Fig. 7(a)	40	0.023	14
Planar carboxyl, Fig. 7(b)	4.7	0.15	14
Planar carboxyl, Fig. 8(a)	32	0.61	1.59
Perpendicular, Fig. 9(a)	1590		
Experimental[a]	5		

[a]Reference 12.

The transmission resonance widths of molecule 1 shown in Fig. 1(c), exhibit both short and long-time scales. The width of the HOMO resonance in Fig. 1(c) is 0.2 meV corresponding to a time τ=3.2 ps. The width of the LUMO resonance, on the other hand, is 0.25 eV corresponding to a time of 2.6 fs. Both the vertical and adiabatic IP and EA are calculated as described in Sec. II D and the results are shown in Table II. For the HOMO level, the adiabatic IP of 6.03 eV is the relevant one. For the LUMO resonance, the vertical EA of 1.60 eV is appropriate. The second vertical ionization potential for both same-spin and opposite-spin calculations is large at 15.02 and 15.17 eV, respectively.

We next calculate an image potential using the 22 nm armchair CNT-vacuum-CNT system, as described in Sec. II C 1. Figure 2(b) shows the converged potential profiles, $\Phi(\vec{r})$ and $\Phi^0(\vec{r})$, plotted along an axial line that lies on top of the CNT contacts and passes through the center of the point charge. The value for the image potential is taken at the position of the point charge $\vec{r}_0$ which is at the center of the HOMO orbital. The DFT-RGF calculation gives an image potential of $\Phi_{CNT}=-0.7$ V. This is also the number obtained from the discretized charge cylinder calculation. As discussed in Sec. II C 1, there is also an image potential resulting from the discontinuity in the dielectric at the SiO_2 interface of $\Phi_d=-0.43$ V. The two image potentials Φ_{CNT} and Φ_d should be calculated self-consistently, since the induced charge in the CNTs will affect the polarization of the dielectric and vice versa. As a zero-order approximation we add the two values together and round down to estimate a total image potential of approximately −1 V. Converting to energy, this gives a +1 eV correction to the HOMO level obtained from the calculated IP. Adding this correction to the HOMO energy of −6.03 eV obtained from the adiabatic IP, we obtain a renormalized value for the HOMO energy of $E_{HOMO}=-5.0$ eV. To give a sense of the uncertainty in this estimate, recall that the absolute mean (maximum) PBE errors in the calculation of the IP found in the study of small molecules were 0.16 eV (0.5 eV).[49]

TABLE II. Calculated ionization potentials and electron affinities of the planar molecule of Fig. 3 using PBE (GGA) and the 6-311+$G(3df,2p)$ basis set (Ref. 45). Vacuum level resides at E=0 eV.

Type	IP (eV)	EA (eV)
Vertical	6.14	1.60
Adiabatic	6.03	1.40

Similarly, the CNT work function is not exactly known since experimentally measured values deviate by several hundred meV. The CNT work function is highly dependent on the type of CNTs, experimental conditions and the method of measurement used. Initial studies done using ultraviolet photoemission spectroscopy of single-walled CNT bundles yielded a work function of 4.8 eV.[57] Field emission microscopy techniques of single-wall CNT ropes give a work function at 5.1 eV.[58] Photoelectron spectroscopy measurements report work-function values between 4.95 and 5.05 eV for CNT ropes.[59] Transmission electron microscope measurements of multiwalled CNTs report a work function between 4.6 and 4.8 eV.[60] Photoemission electron microscopy measurements of individual single-wall CNTs report 4.73 eV.[61] Recently, thermionic measurements of single-wall, double-wall, and multiwall individual CNTs result in work functions of 4.7–4.9 eV.[62] All the experimental reports indicate that the CNT Fermi level most likely resides above the molecular HOMO energy, however exact work-function measurements of individual single-wall CNTs deviate by as much as 200 meV.

To determine which level, HOMO or LUMO, is mediating the transport, we consider the best and worst case alignments of the molecular levels with the CNT Fermi level, allowing the possible values of the CNT Fermi level to range from −5.0 to −4.7 eV. The calculated HOMO level is -5 ± 0.5 eV. Thus, the HOMO can lie in a range of energies from 0.8 eV below the CNT Fermi energy to 0.5 eV above the CNT Fermi energy. Starting with the EA of 1.6 eV and a −1 eV image potential, the renormalized LUMO is at -2.6 ± 0.3 eV using the maximum error in Ref. 49. Therefore, the LUMO lies in a range of energies from 1.8 to 2.7 eV above the CNT Fermi energy. The best case alignment of the LUMO with the CNT Fermi energy is 1 eV further away than the worst case alignment of the HOMO with the CNT Fermi energy. Thus, it is overwhelmingly probable that the transport is mediated by the HOMO.

The calculations presented above indicate that the HOMO resonance is narrow both because it is spatially localized away from the leads and also because the amide linkers reduce coupling between the CNT π orbital and the HOMO of conjugated molecules. The HOMO resonance is also near the CNT Fermi level, but the exact position cannot be predicted accurately enough for quantitative transport calculations. Therefore, we now consider trends and show how the resonance position and width affect the resistance.

To do this, we imitate the experimental measurement conditions as closely as possible, and we consider an ideal Lorentzian transmission spectrum, $T(E)=\frac{\Gamma^2/4}{(E-E_{HOMO})^2+\Gamma^2/4}$. We vary the energetic position, E_{HOMO}, and the width, Γ, and

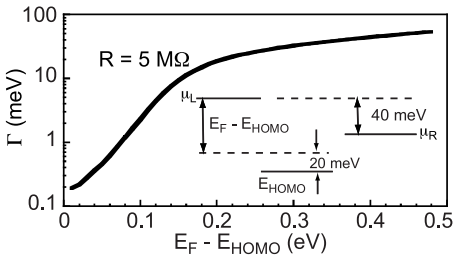

FIG. 10. 5 MΩ equal-resistance contour in the $\Gamma-(E_F-E_{HOMO})$ plane resulting from a Lorentzian transmission spectrum. (Inset) Position of the various energy levels used in the calculation.

plot out an equal-resistance contour in the $\Gamma-E_{HOMO}$ plane corresponding to 5 MΩ. Experimentally, a 50 mV source-drain potential is applied while measuring the room-temperature conductance.[12] The measured resistance of the pristine CNT is 1 MΩ, and the measured resistance of the CNT-molecule-CNT is 5 MΩ. Considering a simple voltage divider, and the weak, symmetric coupling of the molecule to the CNT leads, we assume that 40 mV is symmetrically dropped across the two molecule-CNT interfaces so that the energy of the HOMO level is dropped by 20 meV. Therefore, we reduce the equilibrium value of the HOMO level by 20 meV for the calculation of the current and resistance. The various energies are shown in the inset of Fig. 10. The E_F-E_{HOMO} axis in Fig. 10 is the value before the bias is applied. The current is calculated using Eq. (2), and the resistance is then $R=40\ \text{mV}/I+1\ \text{MΩ}$. Note that the resistances calculated in this manner will differ somewhat from those listed in Table I which were calculated by inverting the value obtained from Eq. (3). All resistances are calculated at $T=300\ K$.

Figure 10 shows the 5 MΩ equal-resistance contour in the $\Gamma-(E_F-E_{HOMO})$ plane. For a narrow resonance of 0.2 meV such as the ones that we obtain for many configurations, the resonance must be within 5 meV of the CNT Fermi energy. The width of a Lorentzian resonance lying 100 meV below the CNT Fermi level must be 2.2 meV to result in a 5 MΩ resistance. Such a width is at least a factor of 10 wider than that obtained for all of our structures with symmetric coupling.

Finally, we comment on the other type of resonance that we observed which was not Lorentzian. It was the quadruply split peak at the Fermi level resulting from the interaction of the zigzag surface states with the HOMO of the molecule shown in Fig. 5. For this system, the surface states are likely to be pinned at the Fermi level.[50] In other similar systems that we have studied with diarylethenes, the presence of the zigzag surface states result in a resistance that is relatively insensitive to the position of the molecular HOMO.

IV. CONCLUSION

In summary, we have theoretically modeled transport of an experimentally measured CNT-molecule-CNT system using DFT based approaches combined with NEGF to calculate the transmission spectrum, the ionization potential and the electron affinity of the molecule, and the image potential due to the proximity of the metallic CNT. CNT chirality, cut geometry, and end passivation were investigated. The features in the transmission correspond directly to the features of the isolated molecular orbitals and the surface states of the cut ends of zigzag CNTs. The HOMO resonance lying on the cross arms of the planar molecule provides conductance at low bias that is qualitatively insensitive to the end groups of the cut CNTs, the CNT chirality, the cut angle, connection type or the number of molecular bridges. Quantitatively, however, these factors can modify the resonance width by an order of magnitude giving rise to corresponding changes in the resistance. Furthermore, the cut ends of a zigzag CNT can result in surface states which hybridize with the molecular HOMO state giving a large transmission peak at the Fermi level which results in a significant reduction in resistance (by a factor of 10 for the structures considered here). Calculations of the ionization potential and electron affinity strongly suggest that the conductance is mediated by the HOMO. However, there is a 0.5 eV uncertainty in the quantitative value of the calculated ionization potential. The uncertainty in the work function of the CNT is also larger than $7k_BT$ at room temperature. This uncertainty alone is large enough to prevent quantitative calculations of the current. Therefore, we treat the relative energy of the HOMO with respect to the CNT Fermi energy as a parameter. For all structures which exhibit no evidence of CNT surface states, there is a single resonant peak due to the molecular HOMO which mediates the hole transport. The calculated resonant width for all such structures with symmetric coupling between the leads is less than or equal to 0.22 meV. Approximating this resonance as a Lorentzian, the resonant peak must lie 5 meV below the CNT Fermi level to give a room-temperature resistance of 5 MΩ. For the zigzag structure with CNT surface states pinned at the Fermi level, there will be a transmission peak at the Fermi level resulting from the surface states. Such a structure can have low resistance (<5 MΩ) even though the molecular HOMO level lies considerably further below the CNT Fermi energy.

ACKNOWLEDGMENTS

This work was supported by the NSF (Grant No. ECS-0524501) and the Semiconductor Research Corporation Focus Center Research Program on Nano Materials (FENA).

APPENDIX: CHARGE CALCULATION

To implement the recursive Green's function calculation of the charge, the left, right, and device regions of the structure are partitioned into a series of nonuniform block layers each containing several atomic layers. Block layers $\{-\infty,\ldots,0\}$ lie in the left contact, $\{1,\ldots,N\}$ lie in the device, and $\{(N+1),\ldots,\infty\}$ lie in the right contact. The localized orbital cutoffs determine the minimum block-layer lengths across the system and are chosen such that the nonzero matrix elements only exist between nearest-neighbor block layers. We will refer to "block layers" as simply "layers," and specifically use "atomic layer" to refer to a single atomic layer within a block layer.

We group the matrices into intralayer subblocks $\mathbf{D}_{i,i}$ and interlayer subblocks $\mathbf{t}_{i,i\pm1}$ where the bold font represents a matrix. The size of these matrices is equal to the number of orbitals per atom times the number of atoms in a particular layer. The layer that contains the molecule is typically larger than the layers in the CNT leads, since we have not attempted to partition the molecule into block layers. The off-diagonal interlayer coupling matrices $\mathbf{t}_{i,i\pm1}$ are, in general, rectangular rather than square, since they can couple diagonal blocks of different sizes. Once the matrices are generated, they are saved and recalled as needed within the algorithm.

The number of electrons, n, associated with the orbitals of atom a is

$$n_a = 2\sum_b \sum_{i,j} \int \frac{dE}{2\pi} \mathrm{Im}\{G^<_{i,a;j,b}(E) S_{j,b;i,a}\}. \tag{A1}$$

The indices a and b indicate the atom and i and j represent an orbital. For a charge neutral atom, n_a is the integer number of valence electrons (excluding the core electrons). For example, for a neutral C atom, $n=4$. The quantity n_a in Eq. (A1) is, in fact, the Mulliken charge.[63] An alternative is the Löwdin charge,[64]

$$n_a = 2\sum_{b,b'} \sum_{i,j,j'} \int \frac{dE}{2\pi} \mathrm{Im}\{S^{1/2}_{i,a;j,b} G^<_{j,b;j',b'}(E) S^{1/2}_{j',b';i,a}\}. \tag{A2}$$

The Löwdin charge requires calculating the full matrix $G^<_{j,b;j',b'}$. Banded approximations can be made for $S^{1/2}$, but even if $S^{1/2}$ is approximated as triblock-diagonal, the second off-diagonal blocks of $G^<$ must be calculated. We will see below, that for the Mulliken charge of Eq. (A1), only the triblock-diagonal elements of $G^<$ are required which makes the calculation amenable to the RGF algorithm.

To understand what Eq. (A1) means in terms of the RGF algorithm, we rewrite it using layer indices L,

$$n_{a,L} = 2\sum_{b,L'} \int \frac{dE}{2\pi} \mathrm{Im\ tr}\{\mathbf{G}^<_{a,L;b,L'}(E)\mathbf{S}_{b,L';a,L}\}. \tag{A3}$$

Again the bold font indicates that $\mathbf{G}^<$ and $\mathbf{S}$ are matrices whose size is determined by the number of orbitals associated with atom a in layer L and with atom b in layer L'. The trace is over all the orbitals of atom a in layer L. Since $\mathbf{S}$ is block tridiagonal, we are required to calculate the diagonal blocks and first off-diagonal blocks of $\mathbf{G}^<$. In other words, the calculation of $n_{a,L}$ requires the calculation of $\mathbf{G}^<_{L,L}$ and $\mathbf{G}^<_{L,L\pm1}$.

In the absence of incoherent scattering, the expression for the electron number in layer L, Eq. (A3), can be written as

$$\mathbf{n}_L = 2\int \frac{dE}{2\pi} \mathrm{Re}\left\{ \sum_{L'} \underbrace{[(\mathbf{G}^R_{L,1}\mathbf{\Gamma}_{1,1}\mathbf{G}^{R\dagger}_{L',1})f^{\mathcal{L}} + (\mathbf{G}_{L,N}\mathbf{\Gamma}_{N,N}\mathbf{G}^{R\dagger}_{L',N})f^{\mathcal{R}}]}_{-iG^<_{L,L'}(E)} \mathbf{S}_{L',L} \right\}. \tag{A4}$$

To not overload the subscripts in Eq. (A4), we have kept only the layer indices since those are our main focus. Also, an abbreviated notation is used for the Fermi functions, $f^{\mathcal{L}(\mathcal{R})}=f(E-\mu_{\mathcal{L}(\mathcal{R})})$. Equation (A4) shows that we need the first and last block columns of the retarded Green's function for the electron-density calculation.

We can write Eq. (A4) in another form which only requires the left *or* right connected spectral function and the diagonal plus first off-diagonal blocks of the Green's function. Defining the left and right connected spectral functions as $\mathbf{A}^{\mathcal{L}}_{L,L'} = \mathbf{G}^R_{L,1}\mathbf{\Gamma}_{1,1}\mathbf{G}^{R\dagger}_{L',1}$ and $\mathbf{A}^{\mathcal{R}}_{L,L'} = \mathbf{G}^R_{L,N}\mathbf{\Gamma}_{N,N}\mathbf{G}^{R\dagger}_{L',N}$ and using the fact that the full spectral function is the sum of the left and right spectral functions, Eq. (A4) can be written as

$$\mathbf{n}_L = 2\int \frac{dE}{2\pi} \left\{ \sum_{L'} \left[\underbrace{\mathbf{G}^R_{L,1}\mathbf{\Gamma}_{1,1}\mathbf{G}^{R\dagger}_{L',1}}_{\mathbf{A}^{\mathcal{L}}_{L,L'}(E)} (f^{\mathcal{L}} - f^{\mathcal{R}}) + \mathbf{A}_{L,L'} f^{\mathcal{R}} \right] \mathbf{S}_{L',L} \right\}, \tag{A5}$$

where $\mathbf{A}=\mathbf{A}^{\mathcal{L}}+\mathbf{A}^{\mathcal{R}}$. To obtain the electron number for a specific shell on a specific atom, we simply trace $\mathbf{n}_L$ over the orbitals of that shell on that atom.

We can express the left and right terms in Eq. (A5) as a sum of a nonequilibrium and an equilibrium charge contribution ($n_L=n^{neq}_L+n^{eq}_L$). We separate Eq. (A5) by expressing the full spectral function as $\mathbf{A}_{L,L'}=-2\ \mathrm{Im}[\mathbf{G}_{L,L'}]$ giving us

$$\mathbf{n}^{eq}_L = -2\ \mathrm{Im}\left[\int \frac{dE}{2\pi} \left\{ \sum_{L'} [\mathbf{G}_{L,L'} f^{\mathcal{R}}] \mathbf{S}_{L',L} \right\} \right] \tag{A6}$$

and

$$\mathbf{n}_L^{neq} = 2\int \frac{dE}{2\pi}\left\{\sum_{L'}[\mathbf{A}^{\mathcal{L}}_{L,L'}(E)(f^{\mathcal{L}} - f^{\mathcal{R}})]\mathbf{S}_{L',L}\right\}. \quad \text{(A7)}$$

Since, in this work, we only need the equilibrium charge to calculate the image potential, we only use Eq. (A6).

The integral of Eq. (A6) is performed using a well-known complex contour integral approach.[65–67] The integral begins below the energy of the bottom valence band, follows a semicircular trajectory in the upper half of the complex plane with a maximum imaginary component of the energy of 1 eV, and finishes $10k_BT$ above the Fermi energy. At the Fermi energy, the contour passes below the lowest Fermi pole with an imaginary component of 10 meV such that there are no poles contained within the contour. The temperature is 300 K for this calculation. Denoting the energy points on the complex contour as $E=z=x+iy$, points are chosen such that the points on the left part of the contour with increasing y are aligned with the points on the right part of the contour with decreasing y. This ensures that the sum of the discrete differentials, $\Sigma_j \Delta z_j$, along the line integral is real. The integral is performed using Simpson's rule. For the image-potential calculations presented here, we used a fixed set of 25 points for the semicircle and 15 fixed points $\pm 10k_BT$ from the Fermi energy. The energy points are adaptively distributed for optimum load balancing over multiple processors (MPI-based).

The equilibrium charge density requires the exact diagonal, first column, and first off-diagonal blocks of $\mathbf{G}^R$. These elements are calculated with the RGF algorithm.[68] First we calculate the left and right connected Green's functions using

$$\mathbf{g}^{\triangleleft}_{L,L} = [E\mathbf{S}_{L,L} - \mathbf{H}_{L,L} - \tilde{\mathbf{t}}_{L,L-1}\mathbf{g}^{\triangleleft}_{L-1,L-1}\tilde{\mathbf{t}}_{L-1,L}]^{-1} \quad \text{(A8)}$$

and

$$\mathbf{g}^{\triangleright}_{L,L} = [E\mathbf{S}_{L,L} - \mathbf{H}_{L,L} - \tilde{\mathbf{t}}_{L,L+1}\mathbf{g}^{\triangleright}_{L+1,L+1}\tilde{\mathbf{t}}_{L+1,L}]^{-1}. \quad \text{(A9)}$$

The superscript $\triangleleft$ ($\triangleright$) indicates that the Green's function takes into account everything to the left (right) with coupling to the right (left) set to zero, i.e., $\mathbf{g}^{\triangleleft}_{L,L}$ is the surface Green's function at layer L for the semi-infinite region consisting of layers $\{-\infty, \cdots, L\}$. All Green's functions in Eqs. (A8) and (A9) are retarded Green's functions. Equations (A8) and (A9) begin with the surface Green's functions of the left and right contacts, respectively. The off-block-diagonal coupling matrices are $\tilde{\mathbf{t}}_{L,L'} \doteq \mathbf{t}_{L,L'} - E\mathbf{S}_{L,L'}$.

Next, the exact diagonal blocks of $\mathbf{G}^R$ are calculated from

$$\mathbf{G}_{L,L} = [E\mathbf{S}_{L,L} - \mathbf{H}_{L,L} - \mathbf{U}_{L,L} - \tilde{\mathbf{t}}_{L,L-1}\mathbf{g}^{\triangleleft}_{L-1,L-1}\tilde{\mathbf{t}}_{L-1,L} - \tilde{\mathbf{t}}_{L,L+1}\mathbf{g}^{\triangleright}_{L+1,L+1}\tilde{\mathbf{t}}_{L+1,L}]^{-1}. \quad \text{(A10)}$$

After each block $\mathbf{G}_{L,L}$ is calculated, it is stored, and $\mathbf{g}^{\triangleleft}_{L-1,L-1}$ is discarded. The off-diagonal blocks of G^R are calculated next from

$$\mathbf{G}_{L,L+1} = \mathbf{G}_{L,L}\tilde{\mathbf{t}}_{L,L+1}\mathbf{g}^{\triangleright}_{L+1,L+1},$$

$$\mathbf{G}_{L,L-1} = \mathbf{g}^{\triangleright}_{L,L}\tilde{\mathbf{t}}_{L,L-1}\mathbf{G}_{L-1,L-1}. \quad \text{(A11)}$$

Finally, the first block column of G^R is calculated using

$$\mathbf{G}_{L,1} = \mathbf{g}^{\triangleright}_{L,L}\tilde{\mathbf{t}}_{L,L-1}\mathbf{G}_{L-1,1}, \quad \text{(A12)}$$

which is initiated with $\mathbf{G}_{1,1}$.

The first block column $\mathbf{G}_{L,1}$ and the diagonal blocks $\mathbf{G}_{L,L}$ are then used in Eq. (A5) to obtain the electron number. This electron number from Eq. (A5) replaces Eq. (21) of Ref. 32. The calculation of the resulting Hartree and exchange-correlation potentials is left unchanged in the code and is described in Ref. 32.

After some experimentation, we found that the following boundary conditions resulted in good convergence of the charge and Hamiltonian matrix elements. For the calculation of the Hartree and exchange-correlation Hamiltonian matrix elements, the charge is held fixed at its equilibrium value on the last four atomic layers of each CNT at the left and right ends for all iterations. For the calculation of the charge from Eq. (A5), the Hamiltonian matrix elements on the last eight atomic layers of each CNT are held fixed at their equilibrium value for all iterations.

*nbruque@ee.ucr.edu

[1] M. A. Reed, C. Zhou, C. J. Muller, T. P. Burgin, and J. M. Tour, Science **278**, 252 (1997).
[2] J. Taylor, M. Brandbyge, and K. Stokbro, Phys. Rev. Lett. **89**, 138301 (2002).
[3] P. Damle, A. Ghosh, and S. Datta, Chem. Phys. **281**, 171 (2002).
[4] X. Zhang, L. Fonseca, and A. A. Demkov, Phys. Stat. Solidi B **233**, 70(2002).
[5] J. M. Seminario, L. E. Cordova, and P. A. Derosa, Proc. IEEE **91**, 1958 (2003).
[6] Y. Xue and M. A. Ratner, Phys. Rev. B **68**, 115406 (2003).
[7] P. Damle, T. Rakshit, M. Paulsson, and S. Datta, IEEE Trans. Nanotechnol. **1**, 145 (2002).
[8] G. C. Liang, A. W. Ghosh, M. Paulsson, and S. Datta, Phys. Rev. B **69**, 115302 (2004).
[9] P. Qi, A. Javey, M. Rolandi, Q. Wang, E. Yenilmez, and H. Dai, J. Am. Chem. Soc. **126**, 11774 (2004).
[10] A. C. Whalley, M. L. Steigerwald, X. Guo, and C. Nuckolls, J. Am. Chem. Soc. **129**, 12590 (2007).
[11] X. Guo, A. C. Whalley, J. E. Klare, L. Huang, S. O'Brien, M. L. Steigerwald, and C. Nuckolls, Nano Lett. **7**, 1119 (2007).
[12] X. Guo *et al.*, Science **311**, 356 (2006).
[13] J. He, B. Chen, A. K. Flatt, J. J. Stephenson, C. D. Doyle, and J. M. Tour, Nature Mater. **5**, 63 (2006).
[14] Z. Qian, S. Hou, J. Ning, R. Li, Z. Shen, X. Zhao, and Z. Xu, J. Chem. Phys. **126**, 084705 (2007).
[15] S. H. Ke, H. U. Baranger, and W. Yang, Phys. Rev. Lett. **99**, 146802 (2007).
[16] M. del Valle, R. Gutierrez, C. Tejedor, and G. Cuniberti, Nat. Nanotechnol. **2**, 176 (2007).
[17] W. Ren, J. R. Reimers, N. S. Hush, Y. Zhu, J. Wang, and H. Guo, J. Phys. Chem. C **111**, 3700 (2007).

[18] T. B. Martins, A. Fazzio, and A. J. R. da Silva, Phys. Rev. B **79**, 115413 (2009).
[19] S. Y. Quek, L. Venkataraman, H. J. Choi, S. G. Louie, M. S. Hybertsen, and J. B. Neaton, Nano Lett. **7**, 3477 (2007).
[20] S. Y. Quek, J. B. Neaton, M. S. Hybertsen, E. Kaxiras, and S. G. Louie, Phys. Rev. Lett. **98**, 066807 (2007).
[21] H. J. Choi, M. L. Cohen, and S. G. Louie, Phys. Rev. B **76**, 155420 (2007).
[22] J. B. Neaton, M. S. Hybertsen, and S. G. Louie, Phys. Rev. Lett. **97**, 216405 (2006).
[23] H. Basch, R. Cohen, and M. A. Ratner, Nano Lett. **5**, 1668 (2005).
[24] U. Salzner, J. B. Lagowski, P. G. Pickup, and R. A. Poirier, J. Comput. Chem. **18**, 1943 (1997).
[25] C. G. Zhan, J. A. Nichols, and D. A. Dixon, J. Phys. Chem. A **107**, 4184 (2003).
[26] G. Zhang and C. B. Musgrave, J. Phys. Chem. A **111**, 1554 (2007).
[27] J. Li, G. Speyer, and O. F. Sankey, Phys. Rev. Lett. **93**, 248302 (2004).
[28] M. Koentopp, C. Chang, K. Burke, and R. Car, J. Phys.: Condens. Matter **20**, 083203 (2008).
[29] C. Toher and S. Sanvito, Phys. Rev. Lett. **99**, 056801 (2007).
[30] J. Ulrich, D. Esrail, W. Pontius, L. Venkataraman, D. Millar, and L. H. Doerrer, J. Phys. Chem. B **110**, 2462 (2006).
[31] O. F. Sankey and D. J. Niklewski, Phys. Rev. B **40**, 3979 (1989).
[32] A. A. Demkov, J. Ortega, O. F. Sankey, and M. P. Grumbach, Phys. Rev. B **52**, 1618 (1995).
[33] O. F. Sankey, A. A. Demkov, W. Windl, J. H. Fritsch, J. P. Lewis, and M. Fuentes-Cabrera, Int. J. Quantum Chem. **69**, 327 (1998).
[34] J. P. Lewis, K. R. Glaesemann, G. A. Voth, J. Fritsch, A. A. Demkov, J. Ortega, and O. F. Sankey, Phys. Rev. B **64**, 195103 (2001).
[35] P. Jelinek, H. Wang, J. P. Lewis, O. F. Sankey, and J. Ortega, Phys. Rev. B **71**, 235101 (2005).
[36] N. A. Bruque, R. R. Pandey, and R. K. Lake, Phys. Rev. B **76**, 205322 (2007).
[37] J. L. Martins, N. Troullier, and S. H. Wei, Phys. Rev. B **43**, 2213 (1991).
[38] A. D. Becke, Phys. Rev. A **38**, 3098 (1988).
[39] C. Lee, W. Yang, and R. G. Parr, Phys. Rev. B **37**, 785 (1988).
[40] J. Harris, Phys. Rev. B **31**, 1770 (1985).
[41] W. M. C. Foulkes and R. Haydock, Phys. Rev. B **39**, 12520 (1989).
[42] M. Galperin, S. Toledo, and A. Nitzan, J. Chem. Phys. **117**, 10817 (2002).
[43] M. P. L. Sancho, J. M. L. Sancho, and J. Rubio, J. Phys. F: Met. Phys. **15**, 851 (1985).
[44] S. Ramo, J. R. Whinnery, and T. V. Duzer, *Fields and Waves in Communication Electronics*, 3rd ed. (John Wiley and Sons, Inc., New York, 1993).
[45] Y. Shao *et al.*, Phys. Chem. Chem. Phys. **8**, 3172 (2006).
[46] W. J. Hehre, R. Ditchfield, and J. A. Pople, J. Chem. Phys. **56**, 2257 (1972).
[47] P. C. Hariharan and J. A. Pople, Theor. Chim. Acta **28**, 213 (1973).
[48] T. Clark, J. Chandrasekhar, G. Spitznagel, and P. von R. Schleyer, J. Comput. Chem. **4**, 294 (1983).
[49] M. Ernzerhof and G. E. Scuseria, J. Chem. Phys. **110**, 5029 (1999).
[50] F. Buonocore, F. Trani, D. Ninno, A. D. Matteo, G. Cantele, and G. Iadonisi, Nanotechnology **19**, 025711 (2008).
[51] A. Hirsch, Angew. Chem., Int. Ed. **41**, 1853 (2002).
[52] A. H. Flood, J. F. Stoddart, D. W. Steuerman, and J. R. Heath, Science **306**, 2055 (2004).
[53] S. S. Jang *et al.*, J. Am. Chem. Soc. **127**, 1563 (2005).
[54] J. Tomfohr and O. F. Sankey, J. Chem. Phys. **120**, 1542 (2004).
[55] M. A. Reed, J. Chen, A. M. Rawlett, D. W. Price, and J. M. Tour, Appl. Phys. Lett. **78**, 3735 (2001).
[56] J. Chen and M. A. Reed, Chem. Phys. **281**, 127 (2002).
[57] S. Suzuki, C. Bower, Y. Watanabe, and O. Zhou, Appl. Phys. Lett. **76**, 4007 (2000).
[58] D. Lovall, M. Buss, E. Graugnard, R. P. Andres, and R. Reifenberger, Phys. Rev. B **61**, 5683 (2000).
[59] M. Shiraishi and M. Ata, Carbon **39**, 1913 (2001).
[60] R. Gao, Z. Pan, and Z. L. Wang, Appl. Phys. Lett. **78**, 1757 (2001).
[61] S. Suzuki, Y. Watanabe, Y. Homma, S. Fukuba, A. Locatelli, and S. Heun, J. Electron Spectrosc. Relat. Phenom. **144-147**, 357 (2005).
[62] P. Liu, Q. Sun, F. Zhu, K. Liu, K. Jiang, Q. Li, and S. Fan, Nano Lett. **8**, 647 (2008).
[63] R. S. Mulliken, J. Chem. Phys. **23**, 1833 (1955).
[64] P. O. Löwdin, J. Chem. Phys. **18**, 365 (1950).
[65] M. Brandbyge, J.-L. Mozos, P. Ordejón, J. Taylor, and K. Stokbro, Phys. Rev. B **65**, 165401 (2002).
[66] A. D. Carlo, A. Pecchia, L. Latessa, T. Frauenheim, and G. Seifert, in *Introducing Molecular Electronics*, Lecture Notes in Physics (Springer, New York, 2005), Vol. 680, pp. 153–184.
[67] A. R. Rocha, V. M. Garcia-Suarez, S. Bailey, C. Lambert, J. Ferrer, and S. Sanvito, Phys. Rev. B **73**, 085414 (2006).
[68] R. Lake, G. Klimeck, R. C. Bowen, and D. Jovanovic, J. Appl. Phys. **81**, 7845 (1997).